HYDRODYNAMICAL SIMULATIONS OF GAMMA RAY-BURSTS FROM INTERNAL SHOCKS IN RELATIVISTIC FIREBALLS

A. PANAITESCU AND P. MÉSZÁROS

Department of Astronomy & Astrophysics, Pennsylvania State University, University Park, PA 16802

ABSTRACT

We simulate the dynamics of the interaction between relativistically expanding spherically symmetric shells using a 1-dimensional hydrodynamic code and calculate spectra and light-curves arising from such collisions by integrating the synchrotron and inverse Compton emission of the shocked gas. The numerical results reflect the most important features observed in Gamma-Ray Bursts: the spectrum exhibits a progressive softening (its break energy decaying exponentially with the 50–300 keV photon fluence), and the pulses that form the burst appear narrower in higher energy bands. Analytical results for the most important physical parameters of the burst are obtained by solving the shock jump conditions for a pair of interacting shells, in the case when both the forward and reverse shocks are relativistic.

Subject headings: gamma-rays: bursts - methods: numerical - radiation mechanisms: non-thermal

1. INTRODUCTION

We consider Gamma-Ray Bursts (GRBs) arising from multiple internal collisions between relativistic shells of cold ejecta expanding into a vacuum. Under typical conditions, such collisions take place well before the decelerating effect caused by an external medium becomes important. The dynamics and energetics of the unsteady outflow leading to internal shocks in an ejecta released, e.g. in a compact merger or collapse event, were outlined in Rees & Mészáros (1994). In this model, the physical conditions determining the energy deposition in the ejecta are not steady during the entire event, resulting in a non-uniform distribution of the bulk Lorentz factors within the ejecta. Faster shells of material catch up with slower ones, leading to the formation of two shocks in each pair of interacting shells. The slower shell is swept up by a forward shock that accelerates it, while the faster ejecta are decelerated by a reverse shock. Both shocks heat the ejecta, give rise to a turbulent magnetic field and accelerate electrons to a power-law distribution. The shocked fluid cools through synchrotron and inverse Compton emission and through adiabatic losses, due to the radial expansion of the ejecta. The radiation received by the observer comes from a small part of the ejecta, that moves almost toward the observer, due to the high Lorentz factor of the emitting fluid. Consequently, the burst seen by the observer is substantially blue-shifted and much shorter than as seen in the co-moving frame of the ejecta.

The average spectra arising from internals shocks in such unsteady winds have been calculated analytically by Papathanassiou & Mészáros (1996) for wide ranges of model parameters (magnetic field and electron acceleration efficiency, wind duration and wind variability timescale, average Lorentz factor of the ejecta). Their results show that burst spectra can extend over many orders of magnitude, from eV to TeV. The spectra calculated by Pilla & Loeb (1998) show a similar wide range of photon energies, and a time evolution characterized by a softening of the spectrum, determined by the electron synchrotron and inverse Compton cooling in the early phase of the burst, and dominated by the pair-cascade process at later times. For reason-

able values of the outflow Lorentz factors and the shock radius, the depletion of high energy photons by pair creation was found to alter the burst spectra at energies higher than the BATSE window. The two radiating processes which cool the electrons have been discussed by Sari & Piran (1997), who derived constraints on model parameters from the required efficiency, observed peak of the spectrum and ratio of the variability timescale to the burst duration and from the condition of optical thinness to pair creation. A detailed parameter search of the properties of time-integrated internal (as well as external) shocks provides constraints on the values of parameters which lead to bursts in the BATSE window (Papathanassiou & Mészáros 1998). Using a code based on the kinematics of the interaction between many shells, Kobayashi, Piran and Sari (1997) calculated the efficiency with which shell collisions convert their bulk kinetic energy into internal energy and, assuming that this is radiated away, obtained a set of bolometric light-curves. In a more elaborate treatment, Daigne & Mochkovitch (1998) studied the temporal and spectral features of the synchrotron emission from a population of electrons altered by the power-law injection at shocks. They found a good agreement between most of their results and the features shown by real bursts: duration-hardness anti-correlation (e.g. Kouveliotou et al. 1993), appropriate temporal asymmetry of pulses (Norris et al. 1996), spectra well fit by the Band function (Band et al. 1993), spectral hardening before a count rate increase (e.g. Bhat et al. 1995), pulse duration – energy dependence consistent with observations (e.g. Norris et al. 1996), and an exponential dependence of pulses peak energy on the photon fluence (Liang & Kargatis 1996). Other features of the real bursts, e.g. the general softening of the spectrum (Ford et al. 1995), are not well reproduced by the results presented by Daigne & Mochkovitch (1998), probably due to the fact that they did not take into account the effects arising from the geometrical curvature of the emitting source or the radiative (synchrotron and inverse Compton) cooling of the electrons.

In this work we investigate some of the most important properties of internal shock bursts, using a 1-dimensional hydrodynamic code suitable for simulating the interaction between perfect fluids, and calculate the light-curve and spectrum of the radiation in the BATSE range emitted by shock-accelerated relativistic electrons, assuming spherical symmetry. In the framework of numerical hydrodynamic calculations we can follow in detail the post-shock time evolution of the electrons due to radiative and adiabatic losses in each cell of the fluid, and integrate the synchrotron output to determine the photon field that is up-scattered by the electrons. We then integrate the emission of the shocked fluid taking into account the dependence of the Doppler boosting on the angle between the radial direction of outflow and the direction toward the observer, and the effect of the shells' curvature on the photon arrival time. The bursts obtained with this time-dependent radiation and hydrodynamic treatment of the shock evolution show features that cannot be accounted for by kinematic treatments, including a softening of the spectrum and other correlations typical of the observed bursts.

2. ANALYTICAL TREATMENT OF THE TWO-SHELL INTERACTION

Before proceeding to a numerical hydrodynamical treatment, it is useful to start with some preliminary analytical insights. The physical conditions inside the shocked shells and the properties of the emitted radiation can be estimated by first calculating the Lorentz factor of the shock that sweeps up a shell during the interaction with another relativistic shell, in the frame of the yet un-shocked part of the shell. This can be done using the shock equations given by Blandford & McKee (1976) and the fact that the flow velocity and pressure in the shocked fluid has the same value on both sides of the contact discontinuity that separates the interacting shells. In the following analytic treatment, the internal pressure of the un-shocked fluid is neglected, therefore it applies only to a pair of cold shells. The effect of the radial expansion during the shells' collision is also neglected, therefore the following results are accurate only for shells so thin that they do not expand significantly before the shocks sweep them. If the two shells expand prior to their interaction in the way prescribed by Mészáros, Laguna & Rees (1993) (see below) then, during the time it takes the shocks to sweep up the ejecta, the radius of shells roughly doubles, therefore the radial expansion cannot be neglected and the following analytic results should be regarded only as approximative.

The inner shell has a co-moving frame density ρ_i and moves at a Lorentz factor Γ_i , while the outer shell has a co-moving density ρ_o and moves at a Lorentz factor Γ_o , lower than that of the inner shell. The collision of the two shells generates two shocks that compress and heat them. If Γ_{sh} denotes the Lorentz factor of the shocked fluid in the lab-frame, then the Lorentz factors $\Gamma'_{sh,i}$ and $\Gamma'_{sh,o}$ of this fluid in the frame of the yet un-shocked parts of the inner and, respectively, outer shell are:

$$\Gamma'_{sh,i/o} = \frac{1}{2} \left(\frac{\Gamma_{i/o}}{\Gamma_{sh}} + \frac{\Gamma_{sh}}{\Gamma_{i/o}} \right) , \qquad (1)$$

or equivalently:

$$\Gamma'_{sh,i} = \frac{x^2 + g^2}{2gx}, \qquad \Gamma'_{sh,o} = \frac{g^2x^2 + 1}{2gx},$$
 (2)

where

$$x \equiv \frac{\Gamma_{sh}}{\sqrt{\Gamma_i \Gamma_o}}, \quad g \equiv \sqrt{\frac{\Gamma_i}{\Gamma_o}} > 1, \quad \frac{1}{g} < x < g.$$
 (3)

The pressure of the shocked fluid around the contact discontinuity can be calculated for each shock:

$$(p_{sh})_{i/o} = (\Gamma'_{sh,i/o} - 1)(\hat{\gamma}\Gamma'_{sh,i/o} + 1)\rho_{i/o}c^2, \qquad (4)$$

where $\hat{\gamma}$ is the adiabatic index of the heated fluid, assumed to be the same on both sides of the contact discontinuity. Using the equality of these pressures and equation (2), one obtains a quartic equation for the lab-frame Lorentz factor of the shocked fluid:

$$\hat{\gamma}(g^4 - Y)x^4 + 2(\hat{\gamma} - 1)g(Y - g^2)x^3 + 2(2 - \hat{\gamma})g^2(Y - 1)x^2 +$$

$$2(\hat{\gamma} - 1)g(g^2Y - 1)x + \hat{\gamma}(1 - g^4Y) = 0, \qquad (5)$$

where $Y \equiv \rho_i/\rho_o$.

Generally, equation (5) can be solved only numerically. Figure 1 shows the Lorentz factors $\Gamma_{sh,i}$ and $\Gamma_{sh,o}$ of the shocked fluid as functions of the ratio of the pre-shock comoving densities for three values of the ratio of the preshock lab frame Lorentz factors. For given parameter g, the $\Gamma'_{sh,i}$ and $\Gamma'_{sh,o}$ curves are symmetric relative to the ordinate, i.e. $\Gamma'_{sh,i}(Y) = \Gamma'_{sh,o}(Y^{-1})$, as it can be shown using equations (2) and (5). It can be seen that, unless $\Gamma_i/\Gamma_o \gtrsim 5$ and either $Y \gtrsim 10^2$ or $Y^{-1} \gtrsim 10^2$, then $\Gamma'_{sh,i/o} < 2$, which implies that the two shocks that sweep the shells (the reverse shock in the inner shell and the forward shock in the outer one) are only mildly relativistic. Figure 1 also shows the efficiency ϵ at which the two shocks convert the shells' kinetic energy into internal, defined as the ratio between the lab-frame internal energy of the shocked gas and the kinetic energy that this gas had before it was swept up by one of the shocks. For given parameters g and Y, the efficiency is constant as long as there is a shock sweeping up each shell. The efficiency of kinetic to internal energy conversion changes after one of the shells has been entirely swept up by one of the shocks; in this case one can calculate the overall efficiency of the interaction from conservation of momentum and energy. The result is:

$$\epsilon = 1 - \left[1 + \frac{\mu}{G} \left(\frac{G-1}{\mu+1}\right)^2\right]^{-1/2} ,$$
 (6)

where $\mu = M_i/M_o$ is the ratio of the shells' masses and $G = g^2 = \Gamma_i/\Gamma_o$ is the ratio of their Lorentz factors.

Analytic solutions of equation (5) can be obtained in the particular case Y=1 or if one makes the assumption that the two shocks are either quasi-newtonian or relativistic, which requires that $\Gamma_i \gtrsim \Gamma_o$ or $\Gamma_i \gg \Gamma_o$, respectively. These solutions are:

$$Y = 1: x = 1, \quad G-1 \ll 1: x = \frac{gy+1}{g+y}, \quad G \gg 1: x = \frac{Gy-1}{G-y},$$

where $y=\sqrt{Y}=\sqrt{\rho_i/\rho_o}$. Once the shock Lorentz factors are known, one can calculate the co-moving internal and rest mass energy density of the shocked fluid, the turbulent magnetic field B, and the minimum electron Lorentz factor γ_m of the power-law distribution in each shocked shell, from where all the important characteristics of the synchrotron and inverse Compton emission can be derived. Some analytical results in this direction are presented in Appendix A, only for the case of

relativistic shocks ($\Gamma_i\gg\Gamma_o$), as this case leads to higher burst efficiency and, thus, is more likely to be encountered in the bursts we observe. For definiteness we consider here the case of two shells that have not undergone any previous collisions, in which case the two unknown pre-shock co-moving densities ρ_i and ρ_o can be correlated with basic burst parameters. The shells expand prior to the their interaction as described by Mészáros et al. (1993): they go through an acceleration phase, coast at constant Lorentz factor, and later start expanding, their lab-frame thicknesses evolving as $r/\Gamma_{i/o}^2$, where r is the radial coordinate. If the slower shell was released a time t_v before the faster one, then the collision takes place at the "interaction radius"

$$r_{int} = 2\Gamma_i^2 \frac{ct_v}{G^2 - 1} , \qquad (8)$$

where the co-moving densities are

$$\rho_{i/o}c^2 = \frac{E_{i/o}}{4\pi r_{int}^3} \,, \tag{9}$$

 E_i and E_o being the kinetic energies of the two shells, therefore $Y = E_i/E_o$.

Equations (A6) and (A7) show that the burst spectrum depends strongly on the Lorentz factors of the two shells, the ratio of their energies, the burst variability timescale, and the electron acceleration efficiency. The dependence on the Lorentz factors and variability timescale arises mainly from the fact that we considered the interaction between shells that have propagated unperturbed until their collision; the results would be different if one or both shells interacted before with other shells, in which case equation (9) does not hold. The spectrum dependence on the ratios of the shells' Lorentz factors and of their energies comes from the hydrodynamics of the interaction.

3. DESCRIPTION OF THE NUMERICAL CODE

The numerical code that we developed contains two major parts: one which simulates the hydrodynamics of the interaction between two relativistically expanding fluids, described by Wen, Panaitescu & Laguna (1997), and one which calculates the emission of radiation from the shocked gases, through synchrotron and inverse Compton processes, and computes the observed spectrum and photon/energy light-curves, described by Panaitescu & Mészáros (1998a,b). The most important features of our calculation of the burst emission are listed below.

Electron distribution and magnetic field intensity. The intensity B of the turbulent magnetic field is parameterized by the fraction ε_{mag} of the internal energy that is stored in the magnetic field. An electron power-law distribution (of exponent -p) is initialized in a grid cell containing shocked fluid when that cell is added to the shocked structure. The addition of a new "shocked" cell is done by the Glimm method that we use to simulate the propagation of the shocks, when the mass of the pre-shock fluid swept-up since the last added cell reaches the mass corresponding to the cell volume and post-shock density determined by the shock jump equations. The minimum electron random Lorentz factor γ_m of the power-law distribution is set by the energy given to leptons after shock heating, taken as a constant fraction ε_{el} of the total internal energy of the newly shocked fluid, and by the fraction ζ of electrons that are picked up by shock acceleration. The electrons are considered decoupled from protons and

magnetic fields after their initial acceleration (i.e. they are not re-energized), and lose energy through emission of synchrotron and inverse Compton radiation and through adiabatic cooling.

Radiative losses. Given the local value of the turbulent magnetic field B and the evolving electron distribution in each shocked cell, at some lab-frame time t, we calculate the synchrotron losses and integrate the emitted radiation over the entire volume of the shocked fluid and over the electron distribution, to calculate the synchrotron radiation energy density at each point in the shocked fluid, necessary for the computation of the inverse Compton losses. The approximations used for a faster numerical calculation of the synchrotron spectrum and inverse Compton losses are given in Appendix B. Also to reduce the computational effort, we do not use the full shape of the synchrotron spectrum when calculating the inverse Compton losses; instead we approximate as monochromatic the synchrotron radiation to be up-scattered, at an intensity-weighted frequency. Further, the spectrum of the up-scattered radiation is approximated as monochromatic, at the peak frequency of the inverse Compton spectrum corresponding to given electron Lorentz factor and to the intensity-averaged synchrotron frequency. Thus we expect that the up-scattered radiation is correctly calculated at frequencies that are not too close to the limits of the inverse Compton spectrum. We checked the correctness of this supposition by calculating burst light-curves using the full shape of the inverse Compton spectrum (which leads to substantially longer runs) and by comparing them with those obtained using the monochromaticity approximations. It is worth stressing here that, for an accurate treatment of the inverse Compton losses, one has to resort to numerics in order to take into account the relativistic beaming of the local synchrotron output, due to the relative motion of the cells where the photons are generated and up-scattered.

Light-curves and spectra. We integrate the synchrotron and inverse Compton emission over the electron distribution, the volume of the entire shocked fluid, and the evolution of the interacting shells, to calculate the observed light-curves and instantaneous/brightness-averaged spectra, taking into account the beaming, Doppler frequency shift and time contraction due to the relativistic motion of the radiating fluid. The relativistic effects are dependent on the angle between the radial direction of outflow and the direction toward the observer. Therefore, assuming that the shells are spherically symmetric at least within the cone of half-angle Γ^{-1} visible to the observer, the integral over volume is a double one (over shocked cells and over the angle relative to the line of sight toward the observer), which makes the burst spectrum and light-curve to be a quadruple integral.

4. NUMERICAL SPECTRA AND LIGHT-CURVES

There are a number of model parameters which affect the burst light-curve in the 100 keV–300 keV range spectrum. To simplify things, we consider here the interaction between two spherically symmetric shells that have fixed $E_i=10^{53}$ ergs, $E_o=2\times10^{52}$ ergs, $\Gamma_i=100$ and $\Gamma_o=50$. The initial kinetic energy of the shells can be much lower if they are emitted within a relatively narrow cone; these values were chosen so that, for a burst located at redshift z=1 and having the low efficiency corresponding to (G=2,Y=5), the fluence in the BATSE window is above $10^{-7}\,\mathrm{erg\,cm^{-2}}$. To maximize the brightness

of the burst we assume that electrons reach equipartition with protons and magnetic fields after shock acceleration: $\varepsilon_{el} = 1/2$.

Equations (A6) and (A7) show that there are only two parameters left that determine the burst spectrum: ε_{mag} , on which the spectral peaks depend only weakly, and ζ , the electron injection fraction, on which the same peaks have a strong dependence. By varying this injection fraction one can study the dependence on it of the relative intensity of the synchrotron and inverse Compton components, and determine those values of ζ that maximize the received flux in the BATSE range. Figure 2 shows the shifting of the burst emission toward higher energies with decreasing ζ , due to the increase of the electron Lorentz factor. For $\zeta > 10^{-2}$ the inverse Compton emission occurs in the Thomson regime and carries most of the burst energy, while for $\zeta \lesssim 10^{-3}$ synchrotron dominates over inverse Compton scattering, as the latter takes place in the Klein-Nishina regime. The extent in frequency of each component is determined by the ratio γ_M/γ_m of the maximum and minimum electron energy of the power-law distribution. The γ_m is determined by ε_{el}/ζ and $\Gamma'_{sh,i/o}$ (eq. [A4]), while γ_M is set by the details of the electron acceleration and its calculation is more ambiguous. An upper limit on it is set by requiring that the radiative cooling timescale is longer than the shock acceleration timescale, a condition that does not alter the shape of the spectrum near its peak unless the injection fraction ζ is less than 10^{-2} . In all other cases shown in Figure 2, we have set $\gamma_M/\gamma_m = 100$, which gives the correct shape of the spectrum at frequencies where most the burst emission lies.

As shown in Figure 2, there may be more than one component that carries a good fraction of the burst emission and each component may extend over a few orders of magnitude in frequency. This suggests that the radiation which falls in the BATSE window could represent in some cases a rather small fraction of the entire emission of the burst. If we also take into account that at most half of the available internal energy can be given to electrons by shock acceleration, it results that the efficiency at which the shells' kinetic energy is transformed into radiation visible to BATSE can easily be one order of magnitude lower than the efficiency of $\sim 10\%$ at which the shocks convert the same kinetic energy into internal (for a study of the latter, see Kobayashi, Piran & Sari 1997). We can draw the conclusion that the overall process that leads to γ -ray emission has an efficiency of few percent or lower (see also Daigne & Mochkovitch 1998, Fenimore et al. 1998). Figure 2 also illustrates the fact that the radiation detected by BATSE can be either synchrotron emission or self-inverse Compton scatterings. The distinction between the two cases could be made through the detection of simultaneous emission at energies well below or above the BATSE range.

Figure 3a shows the spectral evolution of a burst whose BATSE window emission is due to inverse Compton scatterings. The large low energy $(20-50~{\rm keV})$ slope of the spectra shown in Figure 3a is a result of the monochromaticity approximation described in $\S 3$, which was made for numerical reasons. Figure 3b shows the spectral evolution of a synchrotron burst. The shaded curve represents the average spectrum, calculated as an intensity-weighted average of the instantaneous spectra. The curve shown with the thick solid line represents a fit with the Band function (Band et al. 1993) to the average spectrum, in the range $30~{\rm keV}{-}3~{\rm MeV}$. The fit is characterized by $\alpha=-1.14$ (the low energy index), $\beta=-2.38$ (the high energy index) and $E_0=326~{\rm keV}$ (νF_{ν} peaks at $(\alpha+2)E_0=282~{\rm keV}$).

As shown in Figure 3c both bursts exhibit a spectral softening

that can be well approximated as a power-law. It should be noted that this is a good fit if the observer would be able to set T=0 when the inner shell is ejected from the burst progenitor. Obviously, the observer can time the burst only when it begins, in which case the power-law spectral softening would be a bad fit. The result shown in Figure 3c should be understood as following: there is a $T_0 \sim (1/5 - 1/3) T_b$, with T_b being the burst duration, such that, if T were measured from T_0 , then the spectral softening would be a power-law in T. A clearer characterization of the burst softening is illustrated in Figure 3d, which shows the spectral peak decays exponentially with the photon fluence Φ_{23} in the middle BATSE channels, a feature that was observed in real GRBs by Liang & Kargatis (1996). Within our model, the softening of the burst is due to two factors. One is that the shell fluid shocked later is less dense due to the radial expansion, leading to lower internal energy densities in the shocked gas, which, for a constant parameter ε_{mag} , implies lower magnetic fields. Secondly, the radiation emitted by the fluid that moves at larger angles off the line of sight toward the center of expansion (the "central line of sight") is less blue-shifted by the relativistic motion of the source and arrives later at observer than the radiation emitted by the shocked fluid expanding at smaller angles relative to the central line of sight. The Lorentz factor of the shocked fluid does not influence the spectral softening, as it is practically constant during the two-shell interaction.

In calculating the spectra shown in Figures 3a and 3b, we have considered the interaction of two shells in which the ejecta are distributed homogeneously. The general spectral softening is the same if one considers a shell to be a collection of "minishells" moving at the same Lorentz factor, i.e. if the two larger shells have a layered structure. In this case the burst light-curve exhibits pulses associated with each new layer that is shocked (sub-pulse structure). The pulses' fluence depend on the kinetic energies of the mini-shells, while the separation between pulses is determined by the spatial separation between layers. The pulse duration, as well as its shape, are determined by the angular extension of the region visible to the observer (a spherical cap of half-angle opening $\sim \Gamma_{sh}^{-1}$), the thickness of the layer and the electron cooling time-scale.

The light-curve shown in Figure 4a was obtained considering an inner group of layers moving at $\Gamma_i = 100$ and an outer one moving at $\Gamma_o = 50$. The mini-shells in each group have equal masses, corresponding to total shell energies $E_i = 10^{53}$ ergs and $E_o = 2 \times 10^{52}$ ergs, if the ejecta are spherically symmetric. The energy release parameters (see figure caption) where chosen such that the gamma-ray burst is due to synchrotron emission. Figure 4a shows six individual peaks generated by the shocks that sweep six outer layers (in this case the inner mini-shells radiate mostly outside the BATSE range), and the 50 keV-300 keV pulse resulting from the addition of these pulses. In Figure 4b we show the dependence of the shape of the first pulse in the burst shown in Figure 4a on the observing energy. The pulse lasts longer at lower energy, as observed in real GRBs. If the pulse duration is defined by $T_{pulse}^{(i)} = \int_{pulse} (F^{(i)}/F_{max}^{(i)}) dT$, where $F^{(i)}$ and $F^{(i)}_{max}$ are the flux and its maximum value in the *i*-th observing channel, then we find that $T^{(i)}_{pulse} \propto E_i^{-0.19}$, where E_i is the geometric mean of the upper and lower energy limits of channel i. The same dependence is found for the other pulses (Figure 4c), as well as in the case when the radiation in the BATSE range is due to inverse Compton emission. The exponent changes slightly if the FWHM of the pulse is used instead of the integral duration defined above, if one uses the lower or upper limits of each BATSE channel instead of their geometric means, or if the photon fluxes are used instead of the energetic ones. The dependence found by Norris et al. (1996) in real GRBs is $T_{pulse}^{(i)} \propto E_i^{-(0.3 \div 0.4)}$, which is stronger than shown by our numerical bursts.

The usual argument used to explain the observed pulse duration – energy anti-correlation is that the electron synchrotron cooling timescale $t_{sy} \propto \gamma_e^{-1} \propto (h\nu_{sy})^{-1/2}$. Because the synchrotron spectrum of an electron extends over more than just one BATSE channel, the above exponent of 1/2 should be regarded only as an upper limit, which is consistent with observations. However the argument based on the electron cooling ignores the possible contribution of the geometrical curvature of the layer and of its thickness to the pulse duration. The spread in photon arrival time due to the curvature of the shell is $T_{\theta} \sim t/(2\Gamma_{sh}^2)$, where t is the lab-frame time, because the observer receives radiation mainly from the fluid moving within $\theta \sim \Gamma_{sh}^{-1}$ off the central line of sight. If the observer frame electron cooling timescale $T_{sy} \sim t_{sy}/(2\Gamma_{sh}^2)$ exceeds T_{θ} , then the shell radius r=ct and its volume increase significantly during t_{sy} , leading to excessive adiabatic losses and to a lower burst efficiency. Thus, an efficient burst is one where $T_{sy} < T_{\theta}$. Our choice of model parameters ensures that the electrons are radiative, and implies that the pulse duration – energy anti-correlation is not due to the electron cooling¹.

In Figure 4d we show the six pulses that form the burst shown in Figure 4a, as seen in the 50 keV-300 keV band. The fluxes have been normalized to their maxima and the pulses have been aligned at their peaks. It can be noticed that these pulses have a sharp rise and a slow decay and that are more asymmetric than the average pulse shape determined by Norris et al. (1996) for separable pulses in long and bright GRBs. The pulse shape is determined by the relative importance of the layer thickness, its angular spreading and the electron cooling. As mentioned before, for our choice of energy release parameters the electron cooling is too fast to play any part in determining the pulse shape. If the thickness of the layer is not taken into account, then the emitting region is approximated by a surface and the emission of radiation is almost instantaneous. This explains the similarity between the shape of the numerical pulses and that obtained analytically by Fenimore, Madras & Nayakshin (1996) for the pulse resulting from the interaction between a single shell and a stationary medium, when the shell is approximated as infinitesimally thin and the radiated power as a delta-function in time. The effect of taking into account the shell thickness can be assessed by comparing the light-curves shown in Figures 4aand 4b, corresponding to a shell containing several thin layers and one infinitesimally thin layer, respectively. Thus, a shell thickness $\sim r/\Gamma^2$ yields a slightly more symmetric pulse, and a shell thickness larger than predicted by Mészáros et al. (1993) is required to obtained an even more symmetric pulse.

The above equation for the spread in the photon arrival time due to the geometric curvature of the source $(T_{\theta} \sim t/(2\Gamma_{sh}^2))$ implies a correlation between the pulse duration and pulse onset time for all the pulses arising from the collision of two inhomogeneous shells. This correlation is illustrated in Figure 4d, which clearly shows that later pulses last longer than earlier ones. However, such a correlation will not be manifested by all

the pulses in a real GRB, as it is possible that pulses seen close to each other by the observer were emitted by different groups of colliding mini-shells, located at different radii, and thus having different durations. This is illustrated in Figure 5, where we considered 10 pairs of interacting shells. Each pair has the same parameters as the two shells that yield the burst shown in Figure 4a, except that the time interval t_v between their ejection differs from pair to pair. Therefore each pair has a different interaction radius. The time elapsed between the ejection of successive pairs is also considered variable. The light-curve shown in the Figure 5a was calculated assuming that, in the frame of the shocked fluid, the emission is concentrated within two cones of solid angle $4\pi/5$ sr directed outward and inward along the radial direction, so that the observer receives radiation from the shocked gas moving only within $\sim \Gamma_{sh}^{-1}/2$ off the central line of sight. This was done in order to reduce the spread in the photon arrival time due to the angular spread of the shell and the pulse overlapping which is present in Figure 4a. A random injection of several groups of shells can be simulated by repeating and superposing the template pulse shown in Figure 5a, corresponding to arbitrary values of the pulse onset time, intensity and duration determined by the value of r_{int} for each pair of interacting shells. We chose for simplicity a periodic shell Lorentz factor and mass distribution in the wind which ensures that each shell suffers only one collision. An example of such a complex light-curve simulation is shown in Figure 5b.

5. CONCLUSIONS

As illustrated by the numerical results shown in the previous section, the observed GRB γ -rays can be due either to the synchrotron emission from shocked ejecta, if the electron injection fraction is small enough (typically around 10^{-2}) to ensure that the accelerated electrons reach high random Lorentz factors, or to the up-scattering of the synchrotron photons, if the electron injection fraction is not far below unity. The particular choice of the shell Lorentz factors used in this work (determined by numerical reasons) has lead to an overall efficiency of converting the initial shell kinetic energy into γ -rays in the range 25 keV-1 MeV that is below 1%. A wider range of Lorentz factors can increase this efficiency. Nevertheless, since only a fraction of the internal energy of the shocked gas can be given to the electrons through shock acceleration, and the spectral emission range of the burst is very broad, the efficiency in a given instrument's range (such as BATSE) can be substantially smaller than that calculated using only the dynamics of the interaction between shells.

The fact that the emission from the gas moving at larger angles relative to the central line of sight arrives later to the observer, and has a softer spectrum than the emission from the fluid flowing at smaller angles, leads to an increase in the pulse duration with decreasing energy. We find that, if the geometrical curvature of the shell were the only factor that determines the pulse duration, then the pulse duration dependence on energy would be $E^{-0.19}$, which is weaker than observed. The pulse duration is also determined by the electron cooling timescale and by the shell thickness. This inconsistency with observations may be due to our choice in the numerical calculations of parameters that led to an electron cooling timescale smaller than that of the adiabatic losses, to maximize the burst efficiency, and to an

¹Because the sweeping up of a layer is simulated through the addition of a single cell of shocked fluid (which is done for numerical reasons), it follows that the duration dependence with energy shown by the numerically simulated pulses is due only to the geometrical curvature of the emitting shell

interaction radius sufficiently large to ensure optical thinness, which led to a spread in the photon arrival time due to shell's curvature dominating that due to its thickness.

A softening of the burst spectrum with time is a natural consequence of the above-mentioned correlation between the angle relative to the observer at which the emitting fluid moves, the arrival time and the hardness of the radiation received, together with the progressive decrease of the turbulent magnetic field intensity due to the radial expansion of the ejecta. The evolution of the break energy of the numerical spectra can be approximated quite well as an exponential in the 50 keV–300 keV photon fluence, for bursts in which either the synchrotron or the inverse Compton emission peaks around 100 keV. The spectrum of the synchrotron burst is well approximated by the Band function.

As shown by Daigne & Mochkovitch (1997), a significant subset of the spectral-temporal correlations observed can be explained within a simple treatment of the kinematics and dynamics of unsteady winds. Here we have shown that in a more complete radiation and hydrodynamical treatment, some of the burst features found by Daigne & Mochkovitch (1997) are qualitatively confirmed, while some quantitative details differ, possibly because of the more detailed physics (including the hydrodynamic treatment) introduced here. In particular, our treatment is able to reproduce an observational feature that previously was not easily obtained, namely a spectral softening in time.

The "kinematic" light-curves calculated by Kobayashi et al. (1997) for internal shocks exhibit a complicated structure, and their bolometric temporal profiles bear a good resemblance to those of real GRBs. Our band light-curves show a similar behavior, and can in addition probe the physical origin of more detailed effects, such as spectral—temporal correlations. In the case where all pulses within a burst arise from one single group of interacting shells, one would expect a correlation between the pulse duration and the time measured from the beginning of the burst. This is due to the fact that, on average, successive collisions within a single group of shells take place at larger radii, and that the pulse onset time and duration are both proportional with the radius where each collision takes place. Obviously, the pulses seen in a real GRB may be due to several groups of

shells interacting at different radii, and thus producing sets of pulses of different durations that overlap and mix, as illustrated in Figure 5b.

Whereas a pulse duration increase with time is the signature of the ejection of closely bunched shells with different Lorentz factors, a lack of continuous correlation between pulse duration and pulse onset time would indicate repeated episodes, stretching over a longer period of time, of ejection of bunches of shells. This may be useful in mapping the injection time-history by the central engine, and perhaps shed some light on the dynamics of the post-collapse or merger-disruption event. For instance, the above correlation (or lack thereof) could be used for testing whether double (or multiple) peaked bursts arise from discrete and separated "events". Examples of such discrete events might be, e.g., the accretion of discrete rings of disrupted matter (or more speculatively, the collapse to a neutron star followed by collapse to a black hole or the collapse of a primary followed by explosive deleptonization of a small mass neutron star companion). Each discrete event would be characterized by the above correlation within the event, which then resets itself at the next event, if they are truly discrete and independent.

The results published so far on the GRBs produced by internal shocks in an unsteady relativistic wind show that this model is able to explain many of the well established properties and correlations observed in real bursts. Further work is necessary to analyze the model features at a more detailed level: numerical results having sufficient temporal resolution would allow a comparison with the other correlations among pulse features (peakedness, asymmetry, width, centroid lag) found by Norris et al. (1996). Such features, as well as the general efficiency, are issues that may need to be addressed within more specific models for the burst progenitor. The advantage of the calculations presented here is that they are independent of any specific model about the primary event, the only requirement being that the central engine produces a sufficiently energetic relativistic wind.

This research was supported in part by NASA NAG5-3801 and NAG5-2857

REFERENCES

Band, D., et al. 1993, ApJ, 413, 281
Bhat, P.N., et al. 1994, ApJ, 426, 604
Blandford, R.D. & McKee, C.F. 1976, Phys. Fluids, 19, 1130
Blumenthal, G.R. & Gould, R.J. 1970, Rev. Mod. Phys., vol. 42, no. 2, 237
Daigne, F. & Mochkovitch, R. 1998, MNRAS, 296, 275
Fenimore, E.E., et al. 1998, ApJ, submitted (astro-ph/9802200)
Fenimore, E.E., Madras, C. D., & Nayakshin, S. 1996, ApJ, 473, 998
Ford, L.A., et al. 1995, ApJ, 428, 620
Kobayashi, S., Piran, T. & Sari, R. 1997, ApJ, 490, 92
Kouveliotou, C., et al. 1993, ApJ, 413, L101
Liang, E. & Kargatis, V. 1996, Nature, 381, 49
Mészáros, P., Laguna, P. & Rees, M.J. 1993, ApJ, 415, 181

Norris, J.P., et al. 1996, ApJ, 459, 393
Panaitescu, A. & Mészáros , P. 1998a, ApJ, 492, 683
Panaitescu, A. & Mészáros , P. 1998b, ApJ, 501, 772
Papathanassiou, H. & Mészáros , P. 1996, ApJ, 471, L91
Papathanassiou, H. & Mészáros , P. 1998, in preparation
Pilla, R. & Loeb, A. 1998, ApJ, 494, L167
Rees, M.J. & Mészáros , P. 1994, ApJ, 430, L93
Rybicki, G.B. & Lightman, A.P. 1979, Radiative Processes in Astrophysics
(New York:Wiley-Interscience)
Sari, R., & Piran, T. 1997, MNRAS, 287, 110
Wen, L., Panaitescu, A. & Laguna, P. 1997, ApJ, 486, 919

A. **RELATIVISTIC SHOCKS:** $\Gamma_I \gg \Gamma_O$

If the shocks are relativistic $(G \gg 1)$, the solution of equation (5) leads to

$$\Gamma'_{sh,i} \sim \frac{1}{2} \left(\frac{G^3}{(G-y)(Gy-1)} \right)^{1/2}, \quad \Gamma_{sh} = \left(\Gamma_i \Gamma_o \frac{Gy-1}{G-y} \right)^{1/2}, \quad \Gamma'_{sh,o} = y \Gamma'_{sh,i},$$
 (A1)

provided that 2/G < y < G/2 (otherwise the shock propagating in the denser shell cannot be considered relativistic). From equation (4) and assuming the adiabatic index $\hat{\gamma} = 4/3$ for a hot gas, the internal energy density in the shocked fluid is

$$e = \sqrt{\rho_i \rho_o} c^2 \left[\frac{G^3 y}{(G - y)(Gy - 1)} \right] , \tag{A2}$$

and, using equations (8) and (9) to derive the pre-shock co-moving densities, the magnetic field can be calculated:

$$B = 9.5 \times 10^{3} \varepsilon_{mag,-1}^{1/2} E_{i,53}^{1/2} \Gamma_{o,2}^{-3} t_{v,0}^{-3/2} \left[\frac{G^{3}}{(G-y)(Gy-1)} \right]^{1/2} [G],$$
 (A3)

where ε_{mag} is a parameter describing the magnetic field strength (see §3) and where the usual notation $A=10^nA_n$ was used. The minimum electron Lorentz factor γ_m of the power-law distribution of shock accelerated electrons is

$$\gamma_{m,i/o} \sim \frac{1}{3} \frac{m_p}{m_e} \frac{\varepsilon_{el}}{\zeta} (\Gamma'_{sh,i/o} - 1) ,$$
 (A4)

where ε_{el} and ζ parameterize γ_m and an electron index p=2.5 was assumed (see §3). Together with equation (A1), equation (A4) leads to

$$\gamma_{m,i} \sim 300 \frac{\varepsilon_{el}}{\zeta} \left[\frac{G^3}{(G-y)(Gy-1)} \right]^{1/2} = \frac{\gamma_{m,o}}{y} . \tag{A5}$$

The observed peaks of the synchrotron and inverse Compton emission are straightforward to calculate:

$$h\nu_{sy,i} = 1.6 \left(\frac{\varepsilon_{el}}{\zeta}\right)^2 \varepsilon_{mag,-1}^{1/2} E_{i,53}^{1/2} \Gamma_{o,2}^{-2} t_{v,0}^{-3/2} \left[\frac{G^5}{(G-y)^2 (Gy-1)}\right] \left[\text{keV}\right] = \frac{h\nu_{sy,o}}{Y} , \tag{A6}$$

$$h\nu_{ic,i} = 140 \left(\frac{\varepsilon_{el}}{\zeta}\right)^4 \varepsilon_{mag,-1}^{1/2} E_{i,53}^{1/2} \Gamma_{o,2}^{-2} t_{v,0}^{-3/2} \left[\frac{G^8}{(G-y)^3 (Gy-1)^2}\right] [\text{MeV}] = \frac{h\nu_{sy,o}}{Y^2}, \tag{A7}$$

assuming that the up-scattering of photons takes place in the Thomson regime.

The lab-frame electron radiative cooling timescale is upper bounded by the synchrotron cooling time

$$t_{sy,i} = 2.9 \left(\frac{\varepsilon_{el}}{\zeta}\right)^{-1} \varepsilon_{mag,-1}^{-1} E_{i,53}^{-1} \Gamma_{o,2}^7 t_{v,0}^3 \left[\frac{(G-y)(Gy-1)^2}{G^4}\right] [s] = y t_{sy,o} ,$$
 (A8)

which is much shorter than the timescale for adiabatic losses $t_{ad} \sim t_{int}$, where, from equation (8), $t_{int} = r_{int}/c \sim 2 \times 10^4 \, \Gamma_{o,2}^2 t_{v,0}$ s. Equation (eq. [A8]) shows that for model parameters that are not far from the chosen scaling values, the synchrotron cooling timescale of the electrons radiating at $h\nu \sim 100$ keV is smaller by four orders of magnitude than the time during which the shock sweeps up the shell, which is of order t_{int} . For the observer, the electron cooling time appears $\sim \Gamma_{sh}^2$ times shorter, due to the motion of the source, and is therefore much smaller than the spread in the photon arrival time due to the shell curvature, which is of order $t_{int}/\Gamma_{sh}^2 \sim t_v$.

B. SYNCHROTRON AND INVERSE-COMPTON EMISSION

Synchrotron emission. The calculation of the synchrotron spectrum is based on a numerical approximation derived from the equations given by Rybicki & Lightman (1979). The synchrotron power per unit frequency $P(\omega)$ (for one electron) is

$$P(\omega) = \frac{3^{5/2}}{8\pi} \frac{P_{sy}}{\omega_c} F\left(\frac{\omega}{\omega_c}\right); \tag{B1}$$

where $P_{sy}=(1/6\pi)\sigma_{Th}cB^2(\gamma_e^2-1)$ is the frequency-integrated synchrotron power (and averaged over the pitch angle), σ_{Th} being the cross-section for electron scattering and γ_e the electron Lorentz factor, and $\omega_c=(3\pi/8)(eB/m_ec)\gamma_e^2$ is the synchrotron frequency (averaged over the pitch angle), with e and m_e the electron charge and mass, respectively. F(u) can be approximated by $F(u)\sim 1.78\,u^{0.297}e^{-u}$ for $10^{-3.5}< u<10^{0.5}$ with a maximum error of 5%. For u such that F(u)>0.5 (i.e. close to the peak of the synchrotron spectrum) this approximation is accurate to better than 1%. At frequencies far from the synchrotron peak, we used the approximations given by Rybicki & Lightman (1979): $F(u)\sim 2.15\,u^{1/3}$ for $u\ll 1$ and $F(u)\sim 1.25\,e^{-u}\sqrt{u}$ for $u\gg 1$.

Inverse Compton scatterings. The peak of the inverse Compton spectrum and the inverse Compton losses are calculated using approximations derived from the equations given by Blumenthal & Gould (1970). The inverse Compton spectrum peaks at the energy ϵ_p given by

$$\epsilon_p = \frac{4q_p \gamma_e^2 \epsilon_0}{1 + (4q_p \gamma_e \epsilon_0 / m_e c^2)} \,, \tag{B2}$$

where ϵ_0 is the energy of the incident photon, and q_p is a factor that depends weakly on $\gamma_e \epsilon_0$. We found that q_p can be approximated with an error below 1% by

$$q_p = \frac{1}{2} + \frac{5.91 \times 10^{-2}}{1 + 0.184v^{1.31}} + \frac{5.09 \times 10^{-2}}{1 + 51.6v^{1.45}};$$
(B3)

with $v \equiv \gamma_e \epsilon_0/m_e c^2$. Equations (B2) and (B3) lead to $q_p = 0.610$ and $\epsilon_p \sim 2.44 \gamma_e^2 \epsilon_0$ in the Thomson regime ($v \ll 1$), and to $q_p = 1/2$ and $\epsilon_p \sim \gamma_e m_e c^2$ in the extreme Klein-Nishina regime ($v \gg 1$). For the inverse Compton power P_{ic} (per electron) we found that the following approximation:

$$\frac{P_{ic}(v)}{P_{ic}^{Th}} \sim \begin{cases} [1 + 7.67 \exp(2.43 \log v)]^{-1} & v \le 1\\ 0.107 v^{-1.07} \exp(-0.569 \log^2 v) & 1 < v < 10^{1.5} \end{cases},$$
(B4)

where $P_{ic}^{Th}=(4/3)\sigma_{Th}cU_{sy}^2(\gamma_e^2-1)$ is the inverse Compton power in the Thomson regime, and U_{sy} the energy density of the photon field that is up-scattered, has a relative error that increases with v, reaching a maximum value of 10% at $v=10^{1.5}$, where $P_{ic}\sim 10^{-3}P_{ic}^{Th}$. The inverse Compton losses are severely reduced by the Klein-Nishina effect at $v>10^{1.5}$ and an accurate treatment of these losses is not necessary.

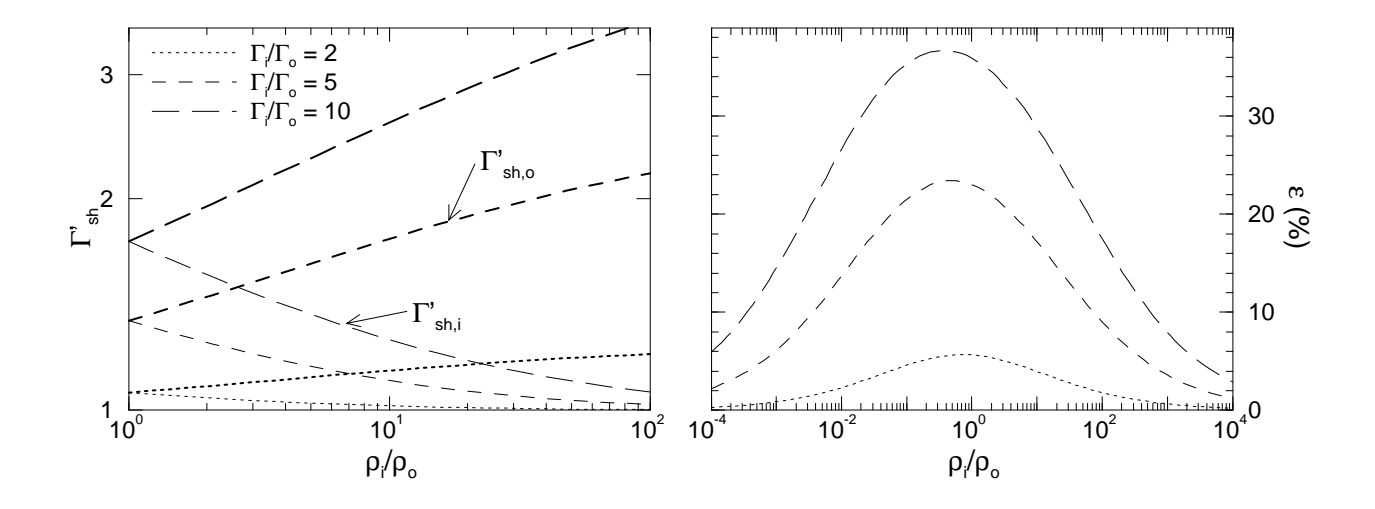


Fig. 1.— Left panel: Lorentz factors of the shocked fluid as measured in the frames of the yet un-shocked gas in the inner shell ($\Gamma'_{sh,i}$ – thin lines) and in the outer one ($\Gamma'_{sh,o}$ – thick lines), for a range of shells' density ratio and for three values of the ratio of their lab-frame Lorentz factors. For given ratio Γ_i/Γ_o , the Lorentz factors $\Gamma'_{sh,i}$ and $\Gamma'_{sh,o}$ are symmetric relative to the ordinate. Right panel: the efficiency of the shocks in converting the shells' total kinetic energy into internal energy. The legend is the same as for the left panel.

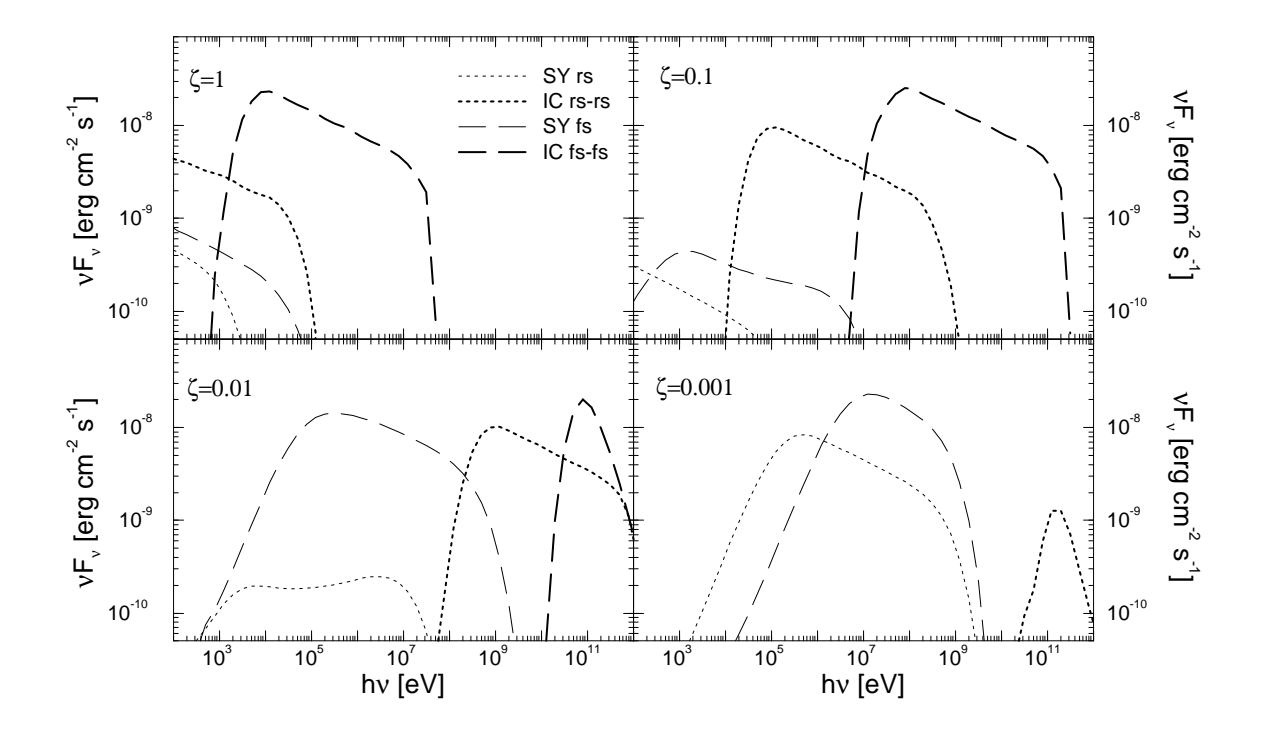


Fig. 2.— Dependence of burst spectra on ζ , the electron injection fraction, for fixed $E_i=10^{53}$ ergs and $E_o=2\times 10^{52}$ ergs in 4π sr, $\Gamma_i=100$, $\Gamma_o=50$, and $t_v=1$ s, $\varepsilon_{el}=1/2$, $\varepsilon_{mag}=10^{-1}$ and p=2.5. The source is located at redshift z=1, with $H_0=75\,\mathrm{km\,s^{-1}Mpc^{-1}}$ and $\Omega=1$. The synchrotron (thin lines) and self-inverse Compton (thick lines) emissions from the reverse shock (rs) and forward shock (fs) are shown separately. The mixed components resulting from up-scattering by one of the shocks of synchrotron photons generated by the other shock are too weak and do not appear in the graphs. Note that for $\zeta\gtrsim 10^{-1}$, the observer receives up-scattered photons in the BATSE range, while for $\zeta\lesssim 10^{-2}$ the γ -ray burst is due to synchrotron emission, and the inverse Compton emission is diminished by the Klein-Nishina reduction.

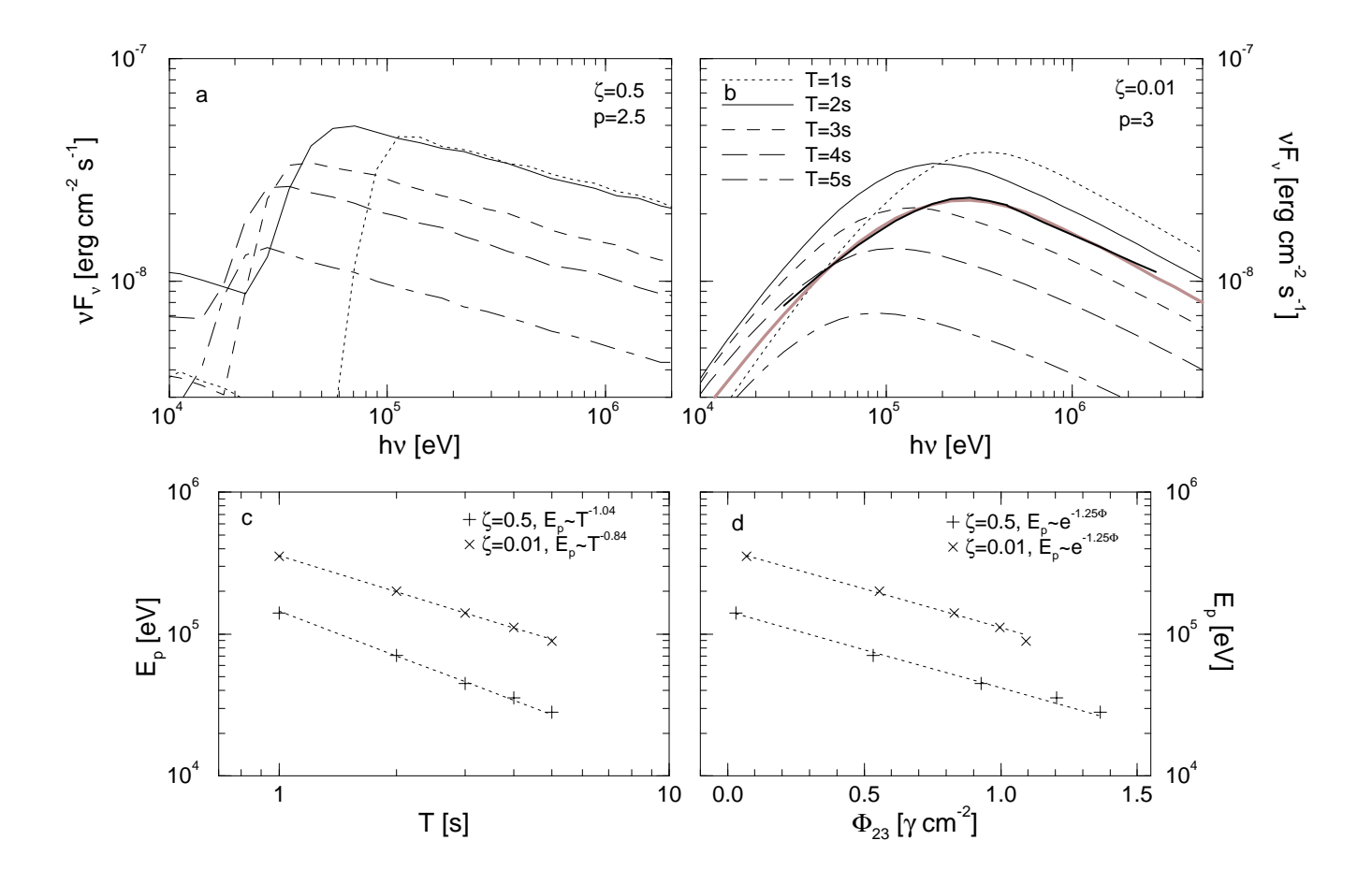


Fig. 3.— Spectral evolution of bursts with same parameters as in Figure 2, except $\zeta=0.5$ for panel a (inverse Compton emission) and p=3 for the panel b (synchrotron emission). The average spectrum shown in graph b with a shaded continuous line is fit in the range 30 keV–3 MeV by the Band function with parameters $\alpha=-1.14$, $\beta=-2.38$ and $E_0=326$ keV. Graph c shows in log-log scale the decrease with time of E_p , the peak of νF_{ν} (power-per-decade), i.e. the softening of the burst spectrum. x's are for synchrotron emission and pluses for inverse Compton radiation in BATSE window. For both types of bursts, a power-law approximates quite well the spectral softening. Graph d shows the exponential decay of the peak E_p with the photon flux Φ_{23} in the range 50 keV–300 keV.

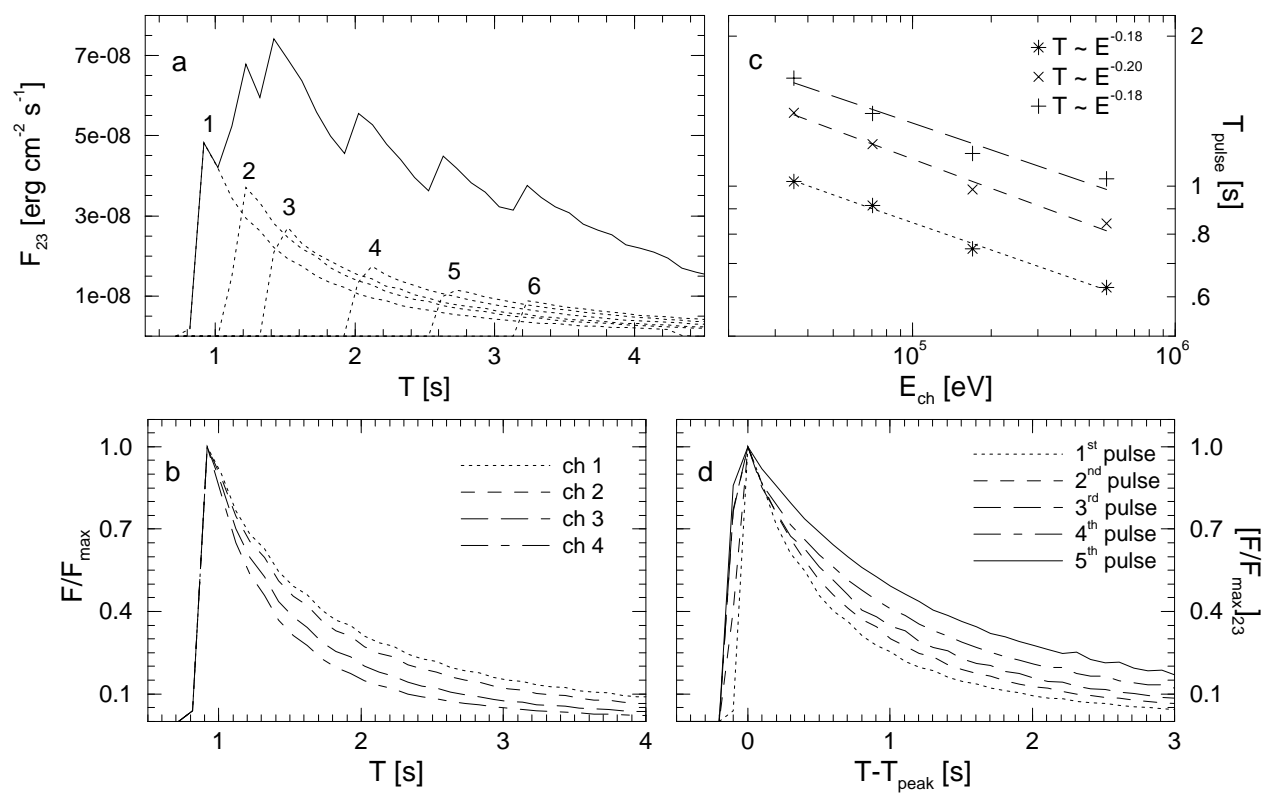


Fig. 4. a: Light-curve of a burst arising from the collision between an inner set of faster and more massive shells with a group of six outer, slower and less massive shells. The Lorentz factor and total kinetic energy of the shells is each group are $\Gamma_i=100$, $E_i=10^{53}$ ergs (assuming spherical symmetry), and $\Gamma_o=50$, $E_o=2\times10^{52}$ ergs. The burst is located at redshift z=1. Other parameters are $\varepsilon_{el}=1/2$, $\zeta=10^{-2}$, $\varepsilon_{mag}=10^{-1}$. b: The first pulse in graph a, as seen in each BATSE channel. The pulse lasts longer at lower energies.

- c: The dependence on observing energy of the duration of the first three pulses shown in graph a.
- d: Evolution of the pulse duration with pulse onset time. For a collision between two layered shells, later pulses last longer than earlier ones.

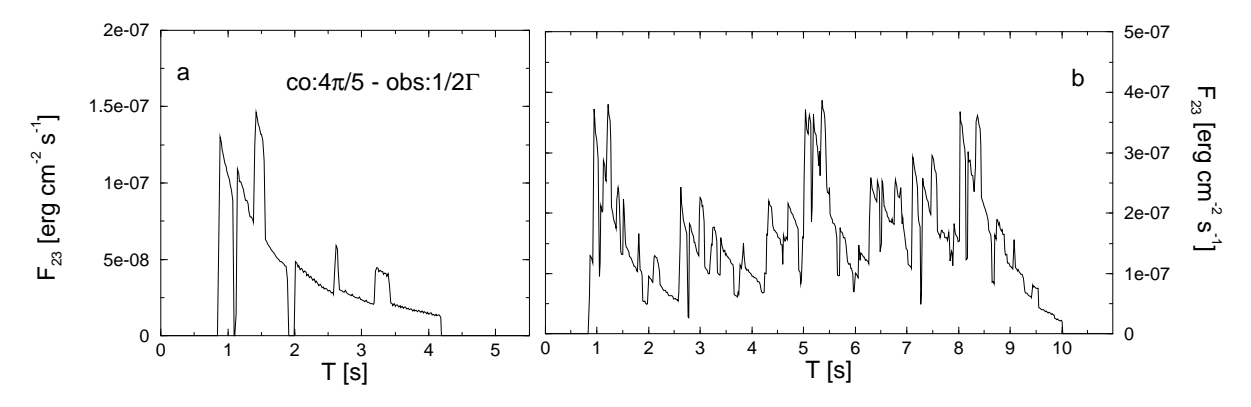


Fig. 5.— Light-curves arising from pairs of shells having the same parameters as the pair that yields the burst shown in Figure 4a, for a pre-beaming factor $4\pi/5$ of the comoving radiation. Panel a shows the pulse from a single pair, while panel b shows the light-curve from a set of 10 pairs (see text for details).